Oxidation of Metals, Vol. 12, No. 1, 1978

The Oxidation Behavior of CoCrAl Systems Containing Active Element Additions

I. M. Allam,* D. P. Whittle,* and J. Stringer*

Received May 1, 1977

The effect of small amounts of yttrium (up to 1 wt.%) and hafnium (up to 1.5 wt.%) on the oxidation behavior of Co–Cr–Al alloys in the temperature range 1000–1200°C for times up to 1000 hr in air has been studied. The major portion of the study has been concerned with Co–10Cr–11Al base alloys. Both isothermal and cyclic tests have been carried out; the cycle used consisted of 20 hr at temperature, followed by cooling to room temperature. Both additions reduce the overall oxidation, Hf somewhat more so than Y. In part, this is due to the improved adhesion between scale and alloy reducing scale spallation at temperature, and in part due to possible modification of the Al_2O_3 grain size. The former factor is far more critical under thermal cycling conditions. Under isothermal conditions the oxidation rate increases with increasing Hf content with all but the 1.5 wt.% alloy oxidizing more slowly than the Hf-free alloy; increase in Y content has the reverse effect. Under thermal cycling conditions the 0.3 and 1.0 wt.% Hf alloys show the lowest overall weight gain. Metallographic evidence suggests that the improved scale adhesion is due principally to a pegging mechanism; the active elements promote the growth of intrusions of Al_2O_3 into the alloy. However, if the intrusions are too large, they can act as initiators of scale failure.

KEY WORDS: CoCrAl; oxidation; oxide scale adherence; rare-earth effect; hafnium; yttrium.

INTRODUCTION

It has been known for over 40 years that the addition of small amounts of active elements to heat-resistant alloys of the Ni–20%Cr or Fe–25%Cr–6%Al type produced a marked improvement in the alloy's behavior in cyclic

*Department of Metallurgy and Materials Science, University of Liverpool, Liverpool, England.

0030-770X/78/0200-0035$05.00/0

oxidation conditions. In the last few years this phenomenon has been widely studied and utilized—the so-called "rare-earth effect." Yttrium has been the most common additive used, although recently it has been shown that fine distributions of a wide range of stable oxides in the alloy have essentially the same effect.

Detailed studies[1–9] of alloys forming Cr_2O_3 indicate that the presence of the active element or stable oxide dispersion in the alloy has the following effects:

i. the amount of chromium required to form a continuous, external Cr_2O_3 scale is reduced;

ii. the growth rate of the scale is reduced, the effect being more marked at higher temperatures;

iii. the transport mechanism in the oxide is changed from predominantly metal transport to predominantly oxygen transport;

iv. the adhesion of the scale is greatly improved, this being particularly noticeable during thermal cycling.

It has not been clearly established whether the effect of adding a reactive element to an alloy is identical to that of adding a stable oxide dispersion. It has been suggested[5] that the oxide dispersion in the alloy nucleates the external scale, thus curtailing the transient stage of oxidation and thereby reducing the tendency of the stable Cr_2O_3 from being disrupted by less stable, but faster-growing oxides. As a consequence, the grain size of the scale is reduced; and it appears that the predominant transport mechanism becomes grain-boundary diffusion of oxygen. In alloys containing reactive element additions only, it is probable that the reactive element oxidizes internally ahead of the scale–alloy interface, but this is unlikely to have any effect in the early stages of oxidation.

A number of mechanistic models have been proposed to explain the improved scale adhesion. The most significant are:

a. Mechanical keying or "pegging" of the scale to the alloy.[10–13] In the case of an active element addition the peg is supposed to be produced by the selective oxidation of the addition at the scale–alloy interface; in the case of the stable oxide dispersion, the fine oxide particles are regarded as the pegs.

b. Provision of sites for vacancy condensation[14] by the internal oxide particles of the active element, or the stable oxide dispersion, thus eliminating interfacial porosity. The vacancies may arise from the scale formation[14] or from a Kirkendall effect in the alloy substrate.[15]

c. Formation of a compound oxide layer[16] between scale and substrate which has a coefficient of thermal expansion that gradually changes from a value similar to that of the alloy to a value close to that of the scale—a graded seal.

d. Modification of the oxide scale plasticity[17] allowing accommodation of the thermally induced stresses.

e. Elimination of the lateral growth of the oxide by incorporation of the yttrium into the scale, which suppresses the diffusion of aluminum and thus greatly reduces or prevents oxide formation within the scale and the development of a convoluted morphology.[18]

Al_2O_3-forming alloys have been studied in less detail. Scale adhesion is also greatly improved, but there appears to be little effect on the isothermal growth rate of the scale.[19] Al_2O_3 scales always grow by grain-boundary transport of oxygen, so there seems to be no change in transport mechanism. Furthermore, the grain size of the oxide is usually so small that nucleation effects are less likely, and no significant change in the aluminum content required to form a continuous external Al_2O_3 scale has been reported.

The most important group of Al_2O_3-forming alloys to which reactive elements are added are the MCrAlY groups of overlay cladding alloys which are widely used for cladding gas turbine blading exposed to severe environments. M is either Fe, Co, or Ni, but it appears that CoCrAlY coatings have significantly better oxidation resistance. Al_2O_3-forming coatings or claddings degrade principally by continual spallation of the surface oxide scale as a result of thermal cycling; the principal role of the Y therefore is to improve the adhesion. Nevertheless, yttrium may not be the best addition for this purpose. Certainly it has a number of disadvantages: The yttrium is usually present as an intermetallic compound at the grain boundaries, and this can result in hot-working problems. The object of the present investigation is to see whether other active element additions are more efficient in enhancing scale adherence, particularly additions which do not form intermetallic compounds.

EXPERIMENTAL

Alloys were prepared by vacuum induction melting from 99.9% pure starting materials, and were vacuum cast into 25 mm square cross section ingots. The outer layers of the ingots were machined off. The selection of alloy compositions was based on the oxide map of the Co–Cr–Al system,[20] and the Co–10Cr–11Al used as the basis material: This forms an external Al_2O_3 scale over the temperature range covered by this study. Both Y and Hf were used as active metal additions. These two elements differ in that the former tends to form an intermetallic Co_3Y, whereas Hf is completely soluble in the alloy at the concentration levels involved. Table I lists the nominal compositions of the alloys: Metallographic analysis confirms that the actual analyses are little different.

Table I. Nominal Compositions and Weight-Gain Data

Alloy composition, wt.%			Weight gain, mg/cm^2				
			Isothermal, 100 hr			Cyclic 9×20 hr = 180 hr	
Base	Hf	Y	1000°C	1100°C	1200°C	1100°C	1200°C
Co–10Cr–11Al			1.05	0.82	2.05		64.54
		0.05	0.37	0.54			49.92
		0.1		0.31			5.98
		0.3	0.52	0.39	0.89		5.38
		1.0	0.28	0.38			4.27
	0.05			0.17			22.42
	0.1			0.23			23.11
	0.3		0.77	0.49	0.79	3.15	3.67
	1.0		0.43	0.67		2.45	4.18
	1.5			1.12			9.17
Co–10Cr–7Al				0.68			127.22
		1.0		0.48			8.15
	1.0			1.06		5.0	39.77
Co–10Cr–5Al				0.73			135.80
		1.0					132.92
	1.0			0.84			151.99
Co–15Cr–8Al			0.48	0.55			85.17
		1.0		0.44			3.85

All samples, of 2–2.5 cm^2 surface area, were used in the as-cast condition. The coupons were cut from the machined ingots, and their surfaces prepared by grinding on metallographic SiC papers to 800 grit, followed by degreasing.

Oxidation experiments were initially carried out in oxygen; no real differences either in the kinetics or the oxide morphologies and compositions between air and pure oxygen were evident, and the remaining experiments were conducted in static air. Isothermal oxidation experiments were conducted using a Sartorius automatic recording microbalance, mounted above a vertical Kanthal-wound resistance furnace. The temperature was controlled to within ±5°C. Test samples were suspended from platinum wire attached to the microbalance and hanging into the mullite reaction chamber, sealed at the bottom to minimize convection currents. The furnace was first heated to the desired temperature, then raised around the reaction chamber. After oxidation, the furnace was lowered and the specimen left to cool to room temperature before careful removal.

It has been noted[18] that at temperatures above about 1000°C oxidation of the platinum suspension wire to volatile PtO_2 can cause significant weight

losses and that this has to be allowed for in the observed oxidation kinetics. In the present experiments, however, using a static atmosphere and a very fine suspension wire with only a short length in the hot zone, this effect should be negligible and would not invalidate the comparisons of oxidation kinetics between the various alloys.

A further factor relating to the loss of platinum from the suspension wire is its possible effect on the stability of the Al_2O_3 scale.[21] Apparently platinum, as the volatile species PtO_2, can be incorporated into the growing Al_2O_3 scale, where it influences the stress-relief mechanism at temperature or reduces oxidation growth stress generation and thus significantly enhances the isothermal stability of the scale. In the present work however, only very minor concentrations of PtO_2 in the atmosphere are anticipated. Furthermore, in the thermal cycling studies detailed below, there was no platinum in the furnace.

Cycling experiments were conducted in a horizontal muffle furnace. Samples were exposed in small recrystallized Al_2O_3 crucibles to collect spalled scale for 20 hr cycles, after which they were allowed to cool for 2 hr before being returned to the furnace. Weight changes were determined at room temperature at the end of each cycle; samples were not removed from the crucibles for weighing and the data presented later include total weight gains, spalled plus adherent oxide.

The surface topography of oxidized samples was examined by electron microscopy after they had been coated by gold sputtering. Scale products were identified by X-ray diffraction. Polished cross sections were studied by optical microscopy and electron probe microanalysis. In some instances scales were stripped from the alloy mechanically by quenching in liquid nitrogen; with more adherent scales the substrate was dissolved away using 10% bromine–methanol solutions. The detached scales were examined in a high-resolution scanning microscope fitted with energy dispersive analysis.

ALLOY STRUCTURE

The Co–Cr–Al alloys consisted of a dark, dendritic phase (β'-CoAl) in a lighter matrix (Co-rich α-phase). Alloys containing yttrium have a third phase,[22] the intermetallic yttride Co_3Y, localized at alloy grain boundaries. However, disappearance of this phase at Y concentrations below 0.1 wt.% suggests that the solubility limit of Y lies somewhere below 0.1 wt.%. Figure 1 shows a typical cross section.

No intermetallic phases were observed in the Hf-containing alloys, which suggests that Hf is completely soluble at least up to 1.5 wt.%. The addition of either element to the alloys reduces the grain size by approximately 50%.

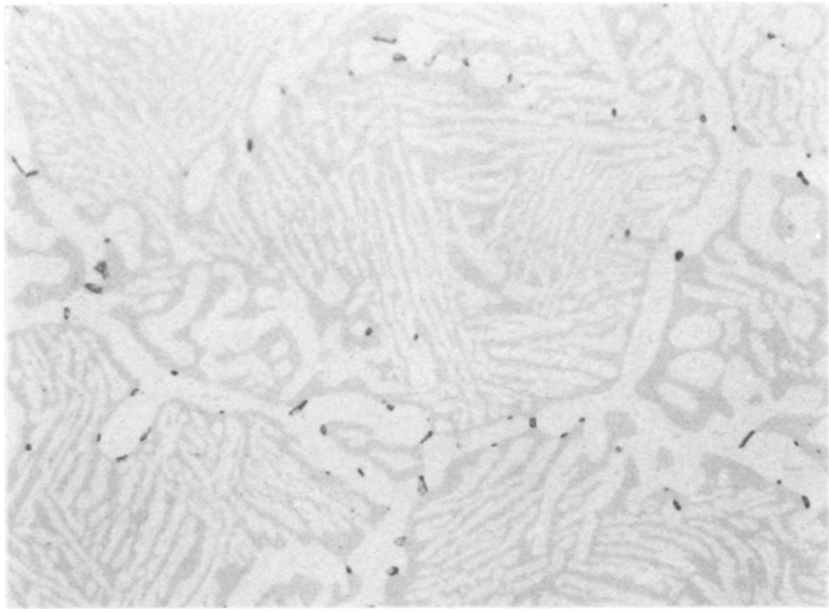

Fig. 1. Cross section of the alloy Co–10Cr–11Al–0.3Y. ×650.

ISOTHERMAL OXIDATION KINETICS

Figure 2 is a direct plot of weight gain per unit surface area vs time during isothermal oxidation at 1100°C of Co–10Cr–11Al containing 0, 0.05, 0.3, and 1.0 wt.% Y. After an initial transient period, an external scale of α-Al_2O_3 is formed on all the alloys with an appropriate reduction in oxidation rate. Increase in alloy Y content resulted in shorter transient periods and a faster attainment of steady-state scaling conditions—continued thickening of the Al_2O_3 scale. This was confirmed by optical microscopy and X-ray analysis of the scales, when it was observed that there was less spinel formed (á distinctive blue color in comparison to the whitish-gray Al_2O_3) on the Co–10Cr–11Al–0.3Y alloy in comparison to the same alloy without Y. Greater amounts of spinel were formed on other alloys (Table I) whose composition approaches the borderline between regions IV and II in the Co–Cr–Al oxide map.[20]

According to Giggins and Pettit,[19] the weight change–time data (or scale thickness–time data) for the growth of Al_2O_3 on CoCrAl, NiCrAl, CoCrAlY, and NiCrAlY alloys could be approximated by a parabolic rate law. However, in the present work this is not the case for the alloys containing Y or Hf. Figure 3 shows a log–log plot of weight change vs time

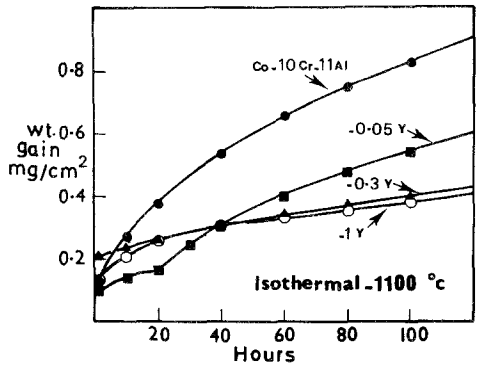

Fig. 2. Isothermal oxidation kinetics at 1100°C of Co–10Cr–11Al containing 0, 0.05, 0.3, and 1.0 wt.% Y.

for the Co–10Cr–11Al–Y alloys at 1100°C. For the Y-free alloys the slopes are close to 0.5; however, for the 0.3Y alloy slopes of 0.21, 0.24, and 0.42 are found at 1000, 1100, and 1200°C, respectively, during the later stages of oxidation. The instantaneous oxidation rate decreases at a much faster rate than is consistent with diffusion-controlled growth.

Table I summarizes the weight-gain data after 100 hr at other temperatures. The weight gain is lower at 1100°C than at 1000°C, but this is because there is a greater weight gain during the initial transient stage at the lower temperature.

Giggins and Pettit[19] also suggested that the presence of Y did not have any significant effect on the growth rate of the Al_2O_3 scale. Furthermore, their data are intermediate between those of the Co–10Cr–11Al alloy, with and without the Y addition in the present study. However, the growth rate of

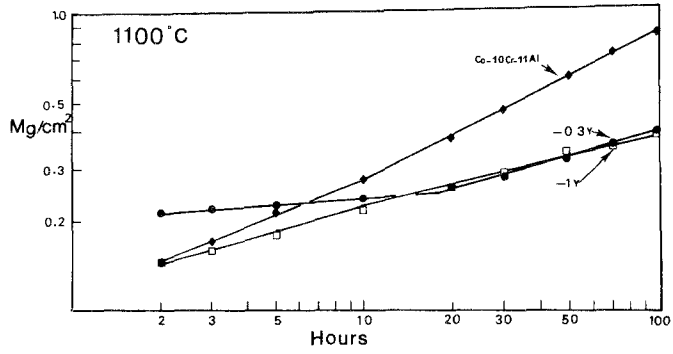

Fig. 3. Log (wt. gain/surface area) vs log (time) for Co–10Cr–11Al and Co–10Cr–11Al–0.3Y oxidized at 1100°C.

Al_2O_3 does appear to be dependent to a limited extent on the alloy composition: Giggins and Pettit's alloys contained 25Cr–6Al–1Y. Figure 4 shows the kinetic curves of a Co–15Cr–8Al alloy with and without Y additions at 1100°C, and it is clear that Y has less effect on the overall rate. This alloy also has a lower overall oxidation rate than the Co–10Cr–11Al alloy, although the two Y-containing alloys behave very similarly.

Figure 5 shows the influence of Hf additions on the isothermal oxidation kinetics at 1100°C of Co–10Cr–11Al. Hf also appears to reduce the initial transient stage of oxidation, as well as decreasing the overall rate. The minimum rate is associated with the lowest Hf additions, 0.05 and 0.1 wt.%. Increasing the Hf content causes increased rates, although up to 1% Hf additions rates are still less than the Hf-free alloy; the 1.5% Hf alloy oxidizes

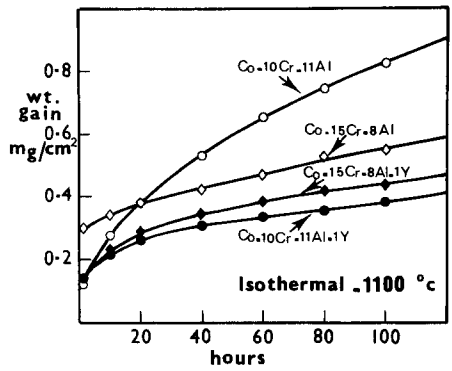

Fig. 4. Isothermal oxidation kinetics at 1100°C of Co–10Cr–11Al and Co–15Cr–8Al with and without a 1.0 wt.% Y addition.

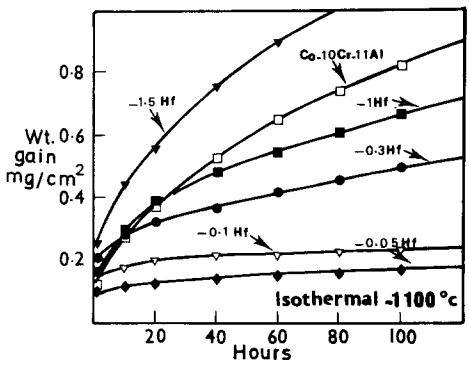

Fig. 5. Isothermal oxidation kinetics at 1100°C of Co–10Cr–11Al containing 0, 0.05, 0.1, 0.3, 1.0, and 1.5 wt.% Hf.

at a faster rate. This behavior is in contrast to that of the Y additions, where the greater the Y content (up to 1 wt.%) the lower the overall weight gain.

Because the rate curves are not parabolic it is not possible to compare the effects of the additions in terms of a well defined rate constant. Figure 6 compares the weight gain after 100 hr exposure at 1100°C. On the active element-free alloys the weight gain ranges from 0.53 to 0.82 mg/cm^2; there is no real systematic variation with alloy composition although the higher chromium content alloys are perhaps slightly better. Y additions of 0.3% or more produce a marginal reduction in the weight gain in comparison with the best Y-free alloy. However, the 0.05 and 0.1 Hf alloys show substantial improvements.

OXIDATION KINETICS DURING THERMAL CYCLING

As indicated earlier, the major effect of the active element additions is in promoting scale–substrate adherence, and this is more critical during thermal cycling tests than during isothermal exposure. Figure 7 shows the weight-change data for the Y-containing alloys during repeated 20 hr cycles at 1200°C. The weight changes include spalled scale which is collected in alumina crucibles and weighed with the samples. In general, increase in the Y content increases the resistance to thermal cycling. Primarily, this is related to the greater number of oxide protrusions penetrating from the scale into the alloy, as will be discussed later. These oxide pegs anchor the scale to the substrate. In addition to improving the adhesion, however, the presence of the active element may also encourage the re-formation of Al_2O_3 after spallation on alloys which in its absence would form spinel or other faster-growing oxides.

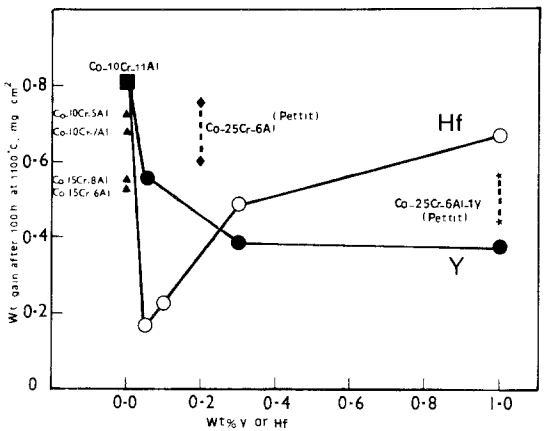

Fig. 6. Weight gain after 100 hr exposure at 1100°C as a function of alloy Hf or Y content: Co–10Cr–11Al alloys.

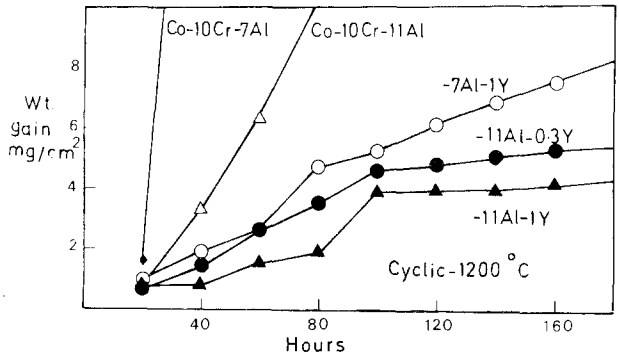

Fig. 7. Weight-gain data for CoCrAlY alloys oxidized at 1200°C under cyclic conditions: 20 hr cycles.

Figure 8 compares the behavior of the Hf-containing alloys, and it is clear that a minimum of 0.3% Hf is necessary to maintain good scale adherence. Alloys containing 0.05 and 0.1% Hf which showed the slowest overall growth rates in isothermal tests behaved little differently than the undoped alloys during thermal cycling. Heavy scaling with these alloys was largely confined to specimen corners and edges where CoO and $CoAl_2O_4$ had been formed following the spallation of the Al_2O_3 scale formed during the first cycle.

Table I summarizes the weight-gain data after nine 20 hr cycles at 1100 or 1200°C of all the alloys studied. Alloys containing 0.3 or 1.0% Hf show the best overall behavior.

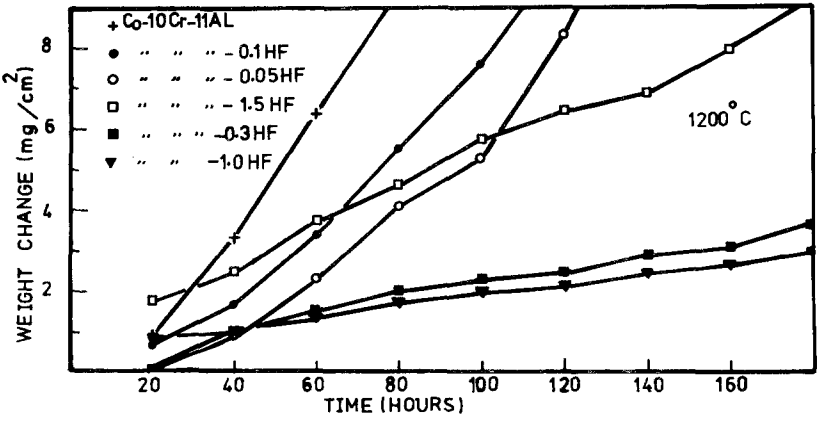

Fig. 8. Weight-gain data for CoCrAlHf alloys oxidized at 1200°C under cyclic conditions: 20 hr cycles.

SCALE AND SUBSTRATE MORPHOLOGIES

Early Stages of Oxidation

Figure 9a shows the underside of the scale spalled from the alloy after 5 min oxidation at 1100°C of a Co–10Cr–11Al alloy; a similar view of the same alloy oxidized for 30 min is shown in Fig. 9b. The Al_2O_3 grain size after 5 min is in the range 0.5–3 μ, while after 30 min it has increased to 1–6 μ. In addition, the scale has apparently a more "open" structure after the longer oxidation time with deep interstices between the Al_2O_3 grains. The alloy surface, where the scale has spalled away, is decorated with numerous voids, Figs. 10a and 10b, many of which appear to coincide with substrate grain boundaries or where scale nodules of the faster growing CoO or Cr_2O_3 have developed (Fig. 10b).

Much the same sort of behavior in these early stages was observed with the Hf- and Y-containing alloys. There were slightly more interfacial voids in the 0.05 Hf alloy than in the 0.05 Y alloy, but in both cases more than in the undoped alloy, Co–10Cr–11Al. Increasing the Hf content to 1.5% produced fewer interfacial voids and correspondingly less scale spallation on cooling after the 5 min exposure at 1100°C. The same was true if the Y content was increased, except in the 1% Y alloy, where there were local high concentrations of interfacial voids. Heavy scale spallation was associated with these areas, while the scale on the remainder of the alloy surface remained tightly adherent.

Later Stages of Growth

Undoped Alloys

Figure 11 shows the surface of the alloy (Co–15Cr–8Al) after spallation of the Al_2O_3 scale during cooling following isothermal exposure. The surface contains numerous smooth areas (about 50% of the interface area) surrounded by rough areas imprinted by oxide grains. Microprobe analysis revealed no compositional differences between the smooth and imprinted areas. The features of the smooth areas suggest they are voids formed during exposure; intimate contact between scale and alloy was maintained only at areas where the oxide imprints are observed on the alloy.

The formation of these voids was observed along the interfaces of all the undoped alloys. In addition, deep substrate grain-boundary valleys were observed in some locations on the Co–10Cr–11Al alloy.

Examination in cross section of the detached Al_2O_3 scale formed on Co–15Cr–8Al shows a graduation in oxide grain size through the section (Fig. 12). The sample has been oxidized for 1000 hr at 1200°C and the total scale thickness is about 20 μ. The oxide grain size in the outer region of the

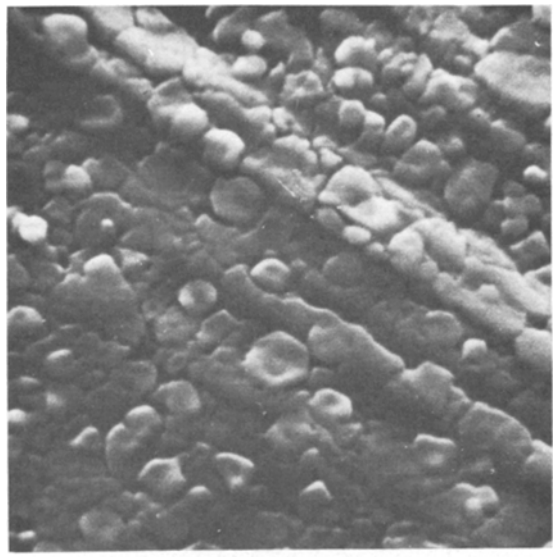

(a)

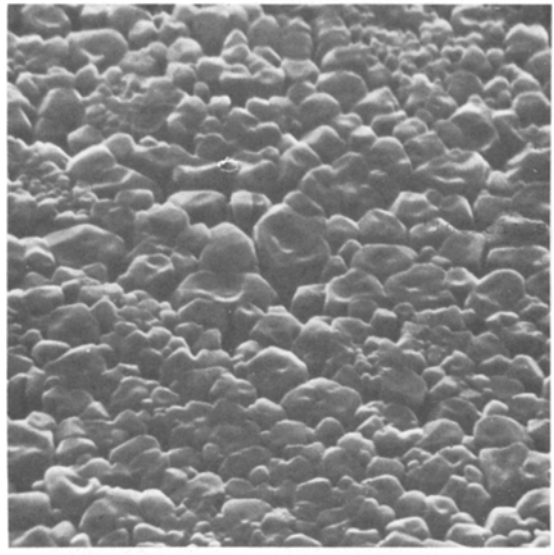

(b)

Fig. 9. Underside of the scale spalled from the surface of Co–10Cr–11Al exposed at 1100°C for (a) 5 min (×3400) and (b) 30 min (×1400); both parts reduced 20% for reproduction.

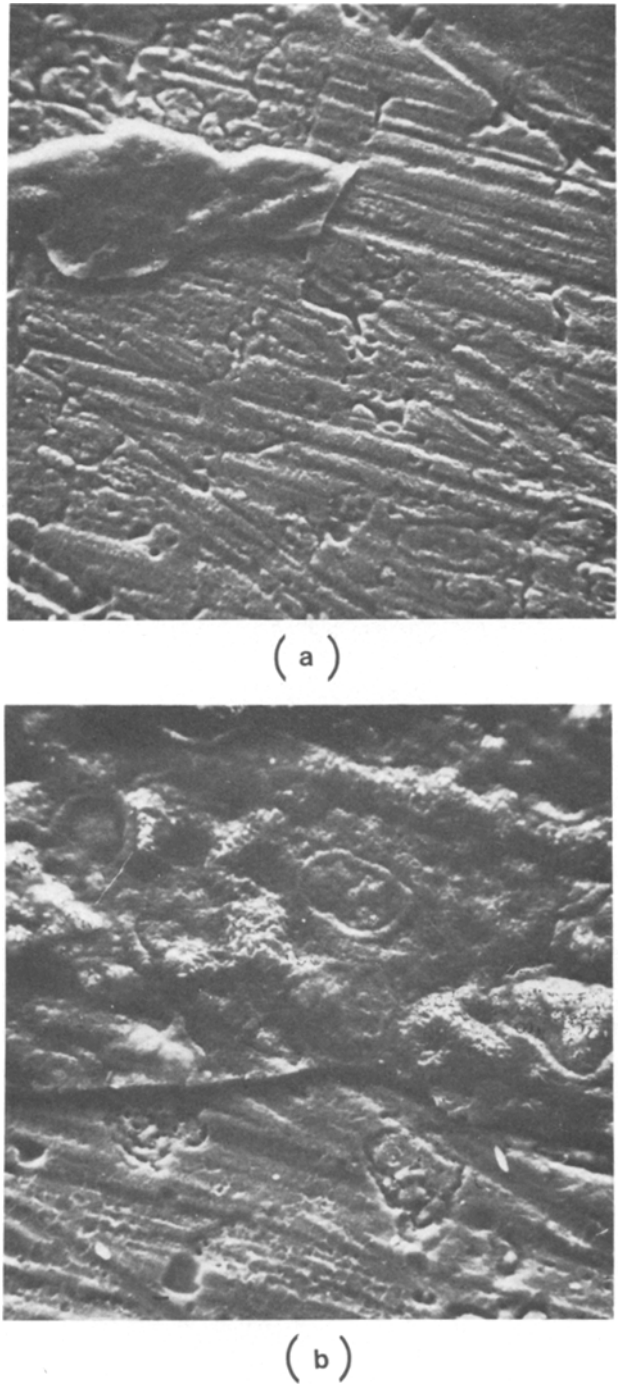

Fig. 10. Surface of Co–15Cr–8Al following scale spallation: samples exposed for 5 min at 1100°C. (a) ×1075; (b) ×2000. Both parts reduced 10% for reproduction.

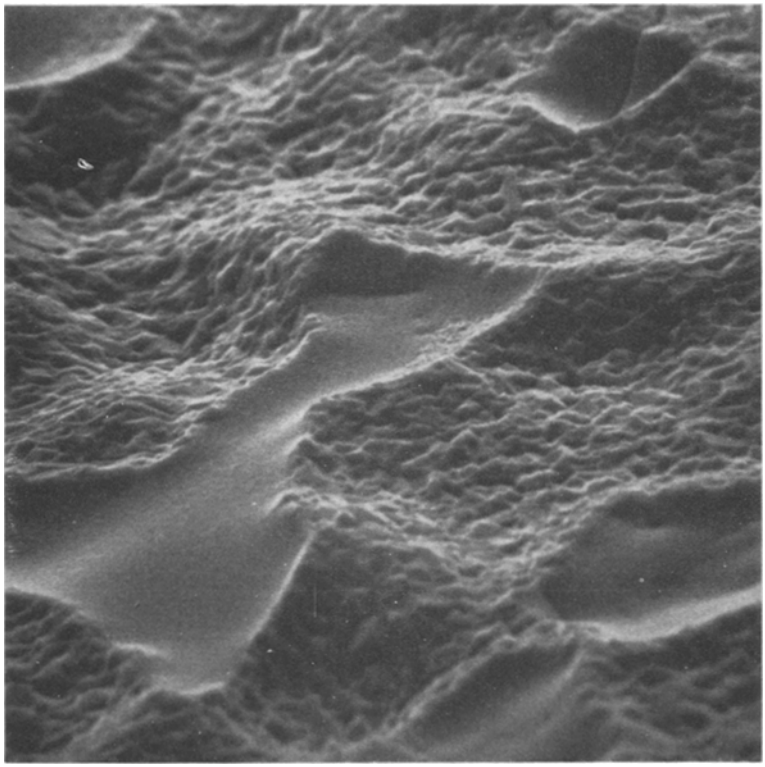

Fig. 11. Surface of Co–15Cr–8Al following scale spallation: Sample exposed for 190 hr at 1200°C. ×1000.

scale is around 0.5 μ, increasing to about 5–10 μ at the inner surface. This gradual increase in Al_2O_3 grain size across the scale appears consistent with a scale growth model of inward oxygen diffusion, new oxide being formed at the oxide–alloy interface. Clearly, there has been no scale breakaway at temperature; otherwise, as will be seen later, there would be new, small-grained Al_2O_3 crystals located within the scale section. Oxide whiskers protruding outwards at the scale–gas interface can also be observed. These whiskers are approximately 0.5 μ in diameter and are also found on similar alloys containing 0.05 and 0.1% Y, but not with alloys of higher Y content. They have been observed previously[15,21] on Al_2O_3 scales, and it was suggested[23] that a dislocation pipe diffusion mechanism was operative. However, whiskers are often associated with compressive growth stresses.[24]

Figure 13 illustrates a further general feature of the inner surface of the Al_2O_3 scales formed on the undoped alloys. Undulations in the outer surface are observed where the oxide grains are somewhat elongated and larger

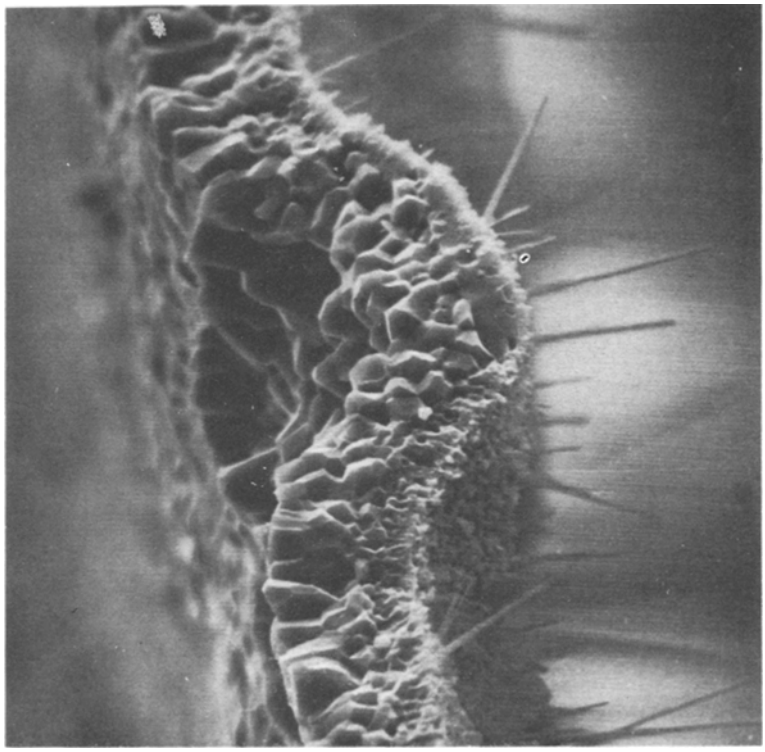

Fig. 12. Cross section of the detached Al_2O_3 scale formed in Co–15Cr–8Al oxidized for 1000 hr at 1200°C. ×1000.

(approximately 10 μ in diameter) than the grains over the remainder of the surface (approximately 3 μ). The total scale thickness at these undulations, which are located above voids at the alloy–scale interface, is similar to that at other locations in the scale, and it is apparent that void formation does not affect the rate of growth of the Al_2O_3. Giggins and Pettit[10] have calculated that evaporation of Al from the alloy is well able to supply Al at the rate demanded by the growing scale. Vapor transport of Al across the voids results in the elongated oxide grain structure; it also results in step-like striations, typical of thermal etching, on the smooth areas at the alloy–scale interface (Fig. 14).

Cracking of the scale or cooling frequently starts along the wrinkles in the outer surface, where the scale is not in contact with alloy. The fracture in the scale corresponds to the boundary between the smooth and imprinted areas on the metal surface; presumably this represents a weak point where the thermally induced stresses during cooling initiate failure.

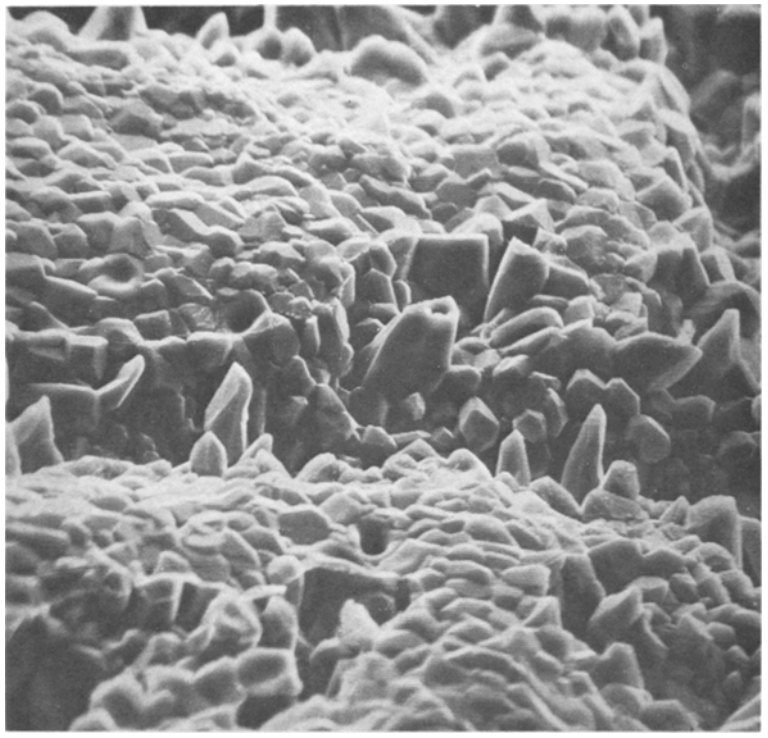

Fig. 13. Surface of the scale formed on Co–15Cr–6Al oxidized for 1000 hr at 1200°C. ×400.

Multiple layers of Al_2O_3 are sometimes formed, particularly on the Co–10Cr–11Al alloy near specimen edges and corners, even during isothermal exposure. The oxide grain size is now relatively fine throughout the section, indicating scale breakaway and re-formation of Al_2O_3 at temperature. In some instances the wrinkled outer portion of the Al_2O_3 encloses a void completely within the scale. However, the fine grain size of the oxide below the void suggests that it was open to the oxidizing environment at some stage, allowing new oxide to be formed beneath the void.

Y-Containing Alloys

The addition of 0.05% Y to the Co–10Cr–11Al base alloy produces little dramatic effect, except that the alloy–scale interface exhibits some undulations. Nevertheless, multilayered Al_2O_3 scales are formed in some areas. The scale spalls profusely from the alloy on cooling, showing large smooth areas (voids) covering about 50% of the interfacial area.

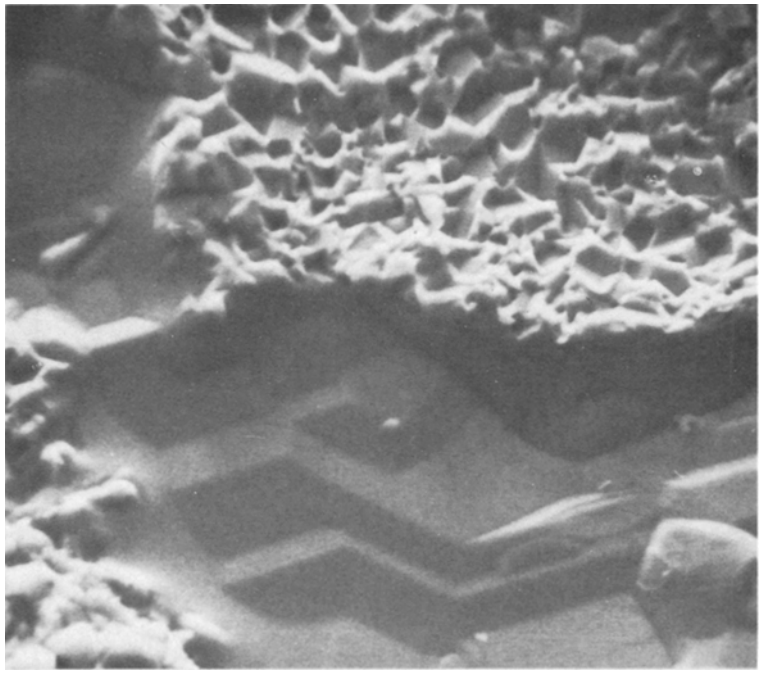

Fig. 14. Alloy surface after scale spallation: Co–15Cr–6Al oxidized for 100 hr at 1100°C. ×1900.

Increase in the Y content of the alloy to 0.1% produces a major change in the interface morphology. No smooth areas are detected, the entire alloy surface being imprinted with oxide grains. Figure 15 shows a Co–10Cr–11Al–01Y alloy oxidized for 1000 hr at 1200°C. The alloy surface in the lower half of the micrograph is imprinted with oxide grains, indicating intimate contact between scale and alloy. Furthermore, even though the scale seems to spall in two discrete layers, an outer, fine-grained layer and an inner, coarser one, there are no signs of separation occurring at temperature.

The other distinctive feature of the Y-containing alloys is the formation of oxide protrusions penetrating into the alloy. Figure 16 shows a typical scale cross section. The protrusions are generally localized at the intersections of substrate grain boundaries with the alloy–scale interface. These are the sites of the Y-rich intermetallic phase in the original alloy, although after oxidation the Y exists as internal oxide. However, following closer examination of Fig. 16 it should be pointed out that the oxide pegs consist primarily of Al_2O_3: The Al_2O_3 has grown preferentially at these points encapsulating the Y-rich internal oxide particles.[25] Energy dispersive analysis of the oxide protrusions (Fig. 17) extending from the underside of the scale confirms the

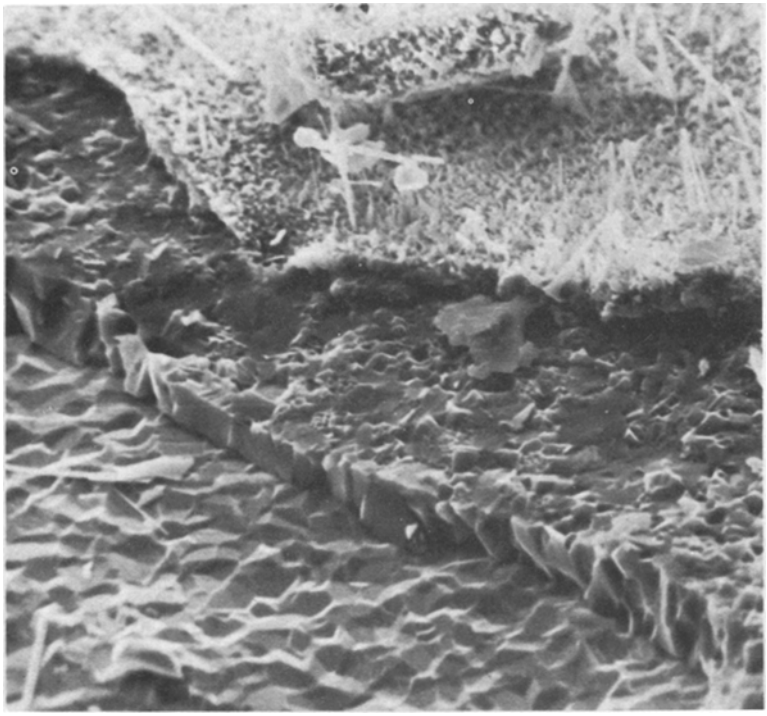

Fig. 15. Alloy surface after scale spallation: Co–10Cr–11Al–0.1Y oxidized for 1000 hr at 1200°C. ×1000.

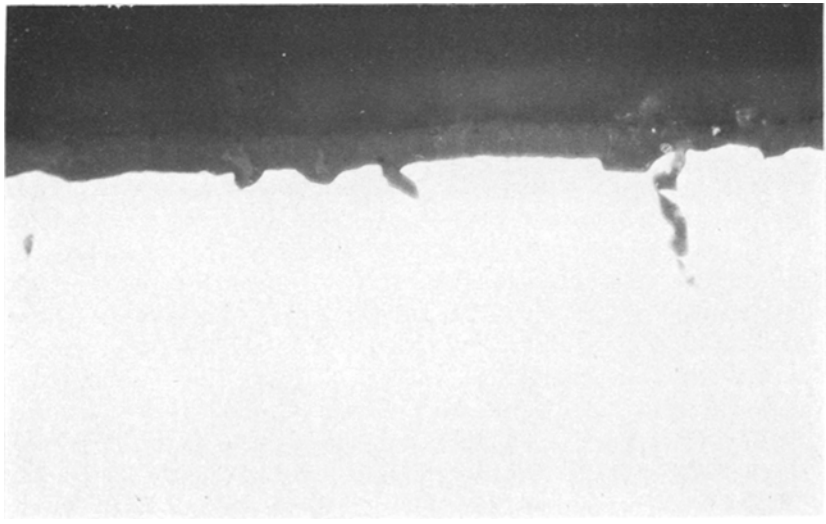

Fig. 16. Cross section of the scale formed on Co–10Cr–11Al–0.3Y oxidized for 130 hr at 1200°C. ×900; reduced 25% for reproduction.

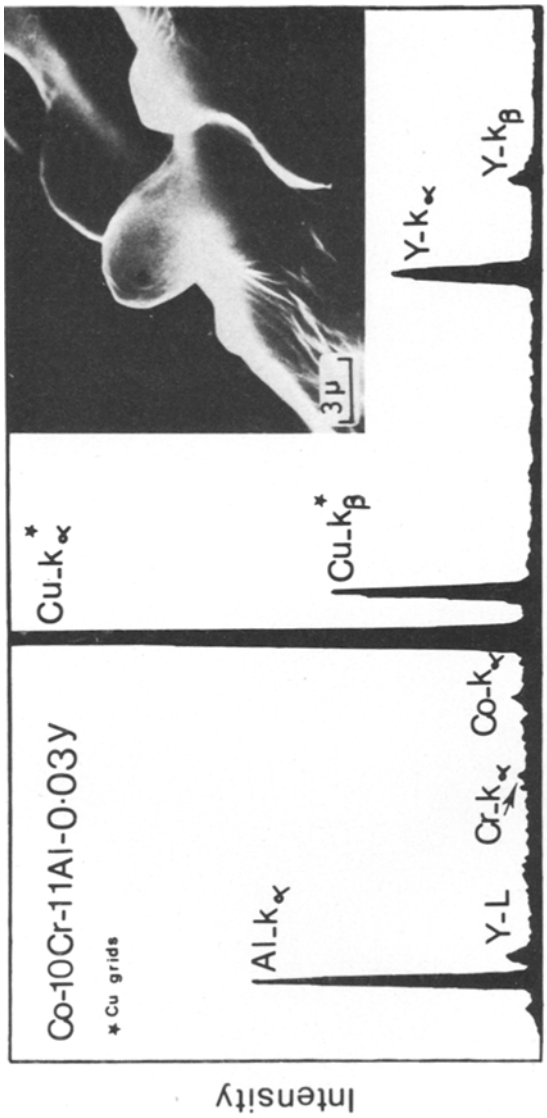

Fig. 17. Underside of the Al_2O_3 scale stripped from the alloy surface: Co–10Cr–11Al–0.3Y oxidized for 75 hr at 1200°C. X-ray energy dispersive analysis is at the tip of one of the oxide protrusions.

Fig. 18. Scales formed on Co–15Cr–8Al–1Y. (a) Cross section of sample oxidized 1000 hr at 1200°C (×750); (b) surface of sample oxidized 1000 hr at 1100°C (×200); (c) surface of sample oxidized 120 hr at 1200°C (×200).

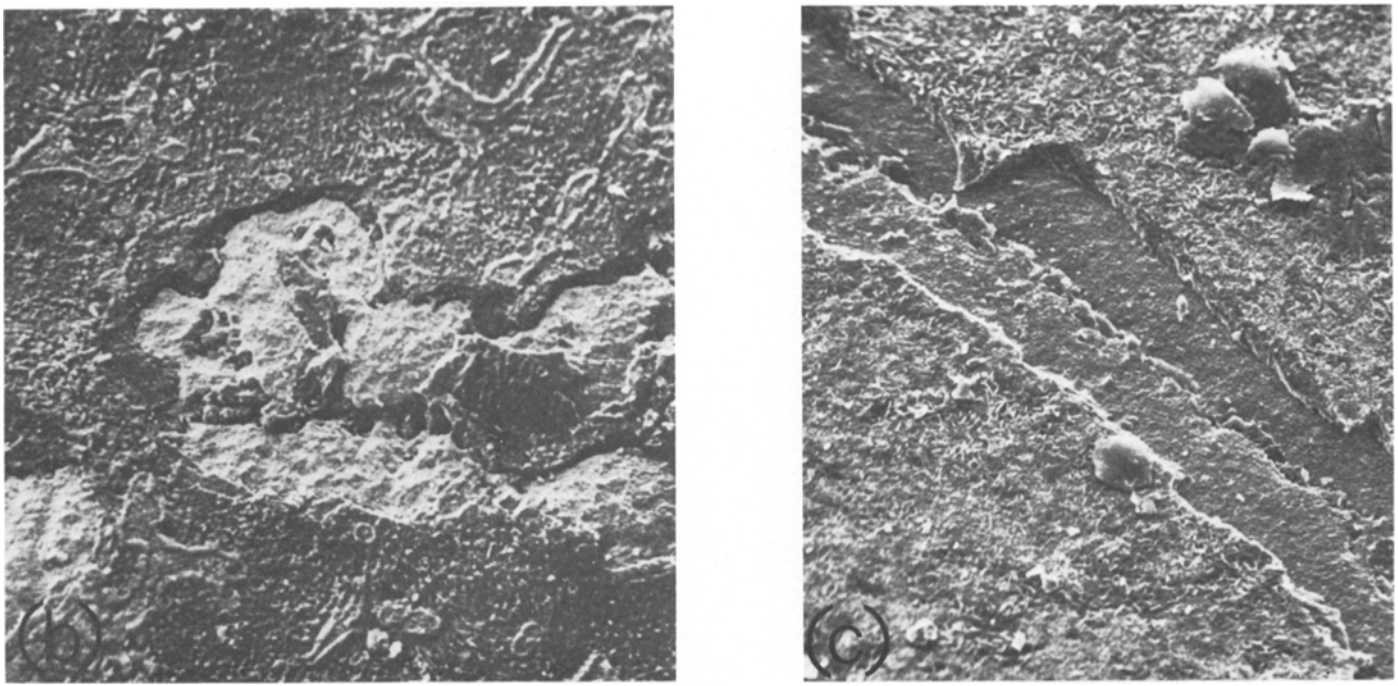

Fig. 18. Continued.

presence of Al and Y; no significant concentration of Y could be detected at other locations.

Further increase in the Y content to 0.3% produces further increases in scale adherence after isothermal exposure, and under thermal cycling conditions as was noted earlier. In comparison to the 0.1% Y alloy, the number of oxide pegs formed at the alloy–scale interface increases; their size remains much the same.

When the Y content is increased beyond the 0.3% level to 1.0%, although the number of oxide protrusions is greater, their size too shows a significant increase. This situation results in a remarkable decrease in Al_2O_3 scale adherence, and frequent spalling takes place during cooling after isothermal tests or during thermal cycling. Scale cracking, when it occurs, initiates above the large protrusions: Figs. 18a and 18b show examples. Equally, aligned protrusions along the substrate grain boundaries can give rise to scale loss at these locations (Fig. 18c). The Al_2O_3 forming the peg is often pulled out from the alloy along with the surrounding scale, as shown in Fig. 19. This may well be related to the relatively smooth interface between peg and alloy as shown earlier in Fig. 17. However, on other occasions, the peg itself breaks near the alloy–scale interface; this was noticed particularly when dissolution of the alloy substrate was necessary to examine the underside of the scale. Figure 20 shows the broken-off stubs remaining. This is to be contrasted with the Hf-containing alloys to be shown later (Fig. 25).

Finally, after relatively long exposures, 1000 hr at 1200°C, of alloys containing lower amounts of Y, 0.3% and less, small voids appear at the alloy surface beneath the surface scale. Figure 21 shows a Co–10Cr–11Al–0.3Y alloy from which the surface scale has been removed. The voids are located at the uppermost part of the boundaries between adjacent oxide grain imprints. The voids are only of the order of 1–2 μ across and are not observed after corresponding exposures of the alloy containing 1% Y.

Hf-Containing Alloys

A 0.05% Hf addition to Co–10Cr–11Al is sufficient to completely eliminate the formation of smooth, voided areas at the alloy–scale interface; only single layers of Al_2O_3 are observed, which are only removed with extreme difficulty to reveal the substrate. Figure 22a shows the highly convoluted outer surface of the scale, but where this has been partially removed (Fig. 22b) it is clear that the scale follows the convoluted surface of the substrate. Equally, the entire alloy surface is imprinted with oxide grains, approximately 4–5 μ in diameter.

Oxide protrusions at the alloy–scale interface start to become noticeable as the Hf content of the alloy is increased. Figure 23a shows the random

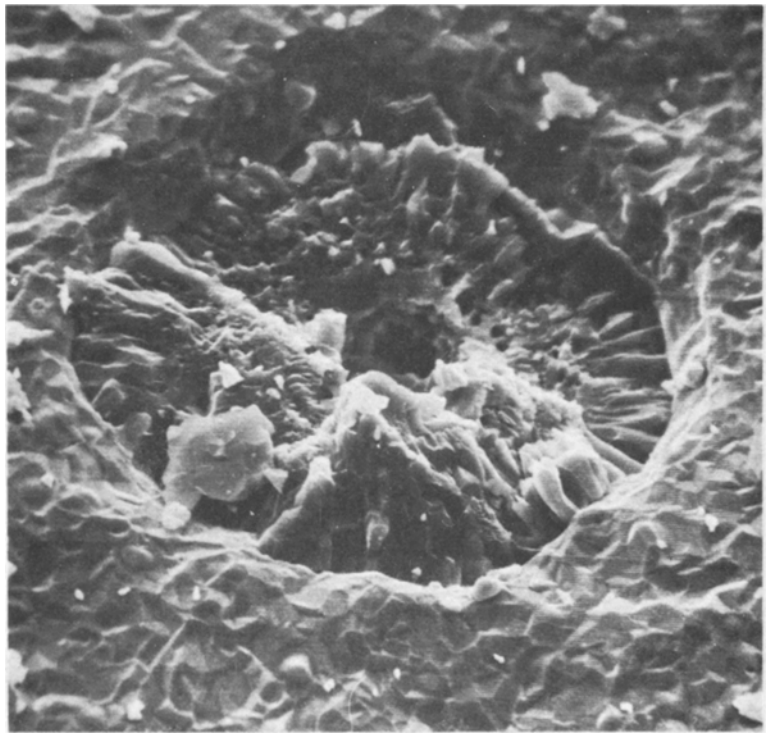

Fig. 19. Surface of the alloy following scale spallation: Co–10Cr–11Al–1Y oxidized for 1000 hr at 1200°C. ×1000.

distribution of pegs occurring at the interface with this alloy, in sharp contrast to the relatively poor distribution of protrusions in the Y-containing alloys. Occasionally, relatively long pegs develop (Fig. 23b) and scale loss is more prevalent above these long pegs. As indicated earlier, the oxide protrusions consist primarily of Al_2O_3, which has grown inwards, encapsulating the Hf-rich oxides formed as an internal oxide precipitate. Electron probe microanalysis (Fig. 24) clearly demonstrates this.

Figure 25 shows the underside of the Al_2O_3 scale formed on Co–10Cr–11Al–1Hf in 1000 hr at 1200°C, after the alloy substrate has been dissolved away. The profusion of inwardly growing pegs is clearly visible, and these clearly provide a better key in anchoring the scale to the substrate than the relatively smooth pegs formed around the Y-rich internal oxides (Fig. 17).

As with the Y-containing alloys, voids re-form at the alloy–scale interface after extended exposures, 1000 hr at 1200°C, on alloys containing 0.1% Hf, but not with alloys of higher Hf content.

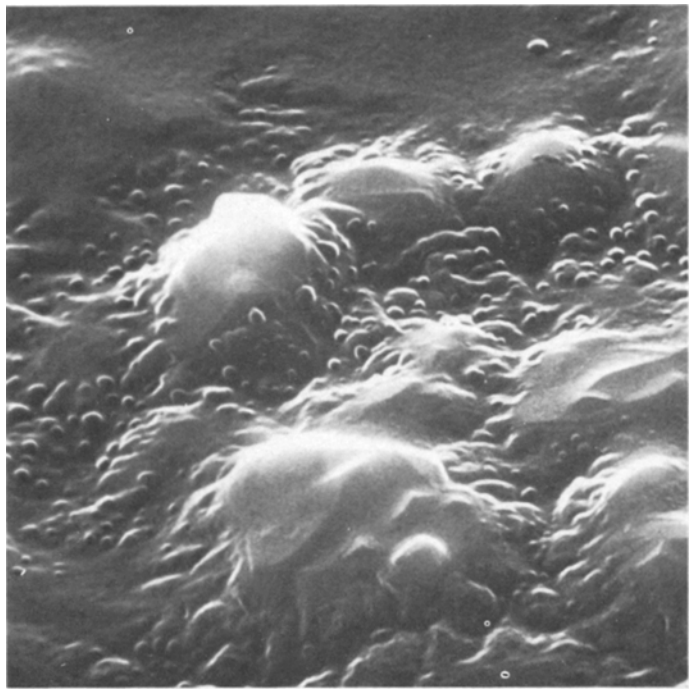

Fig. 20. Underside of the scale stripped from Co–10Cr–7Al–1Y oxidized for 1000 hr at 1200°C; most of the oxide protrusions have broken off. ×5000.

DISCUSSION

The reduction in isothermal growth rate of Al_2O_3 produced by the Y and Hf additions depends on a number of factors. Scale spallation can occur, and while this is not extensive under isothermal conditions, re-formation of Al_2O_3 and the development of multilayered scales can contribute significantly to the weight gain. Differences in multilayer scale formation are thought to be the main reason for the different overall weight gains with the active-metal free alloys. Metallographic evidence shows that multilayered Al_2O_3 scales do indeed sometimes develop on Co–10Cr–11Al samples, particularly near the edges and corners. There was no evidence for this with the 15Cr–8Al alloy, but whether this weight gain really represents the true growth of a single layer of Al_2O_3 on these alloys is not entirely clear. Certainly, under isothermal conditions, scale spallation and re-formation are not excessive, and are not detected in the kinetic curves, nor is there any real departure from parabolic behavior.

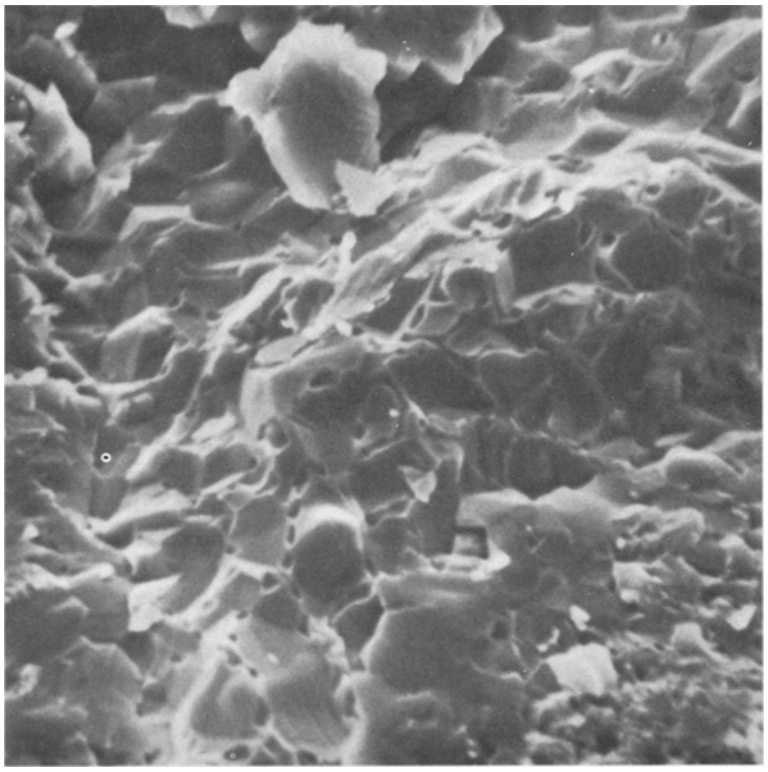

Fig. 21. Alloy surface following scale spallation: Co–10Cr–11Al–0.3Y oxidized for 1000 hr at 1200°C. ×4500.

The results of the thermal cycling tests clearly demonstrate that Y or Hf reduces scale spallation, and under the relatively mild conditions of isothermal exposure multilayer scale formation has probably been entirely eliminated. However, it would appear that the beneficial effects of Y (0.3 wt.% and above) and Hf (less than 0.3 wt.%) go beyond this, and actually reduce the growth rate of the Al_2O_3, in addition to preventing any scale loss. Hf also seems to be the more effective.

The minimum growth rate of Al_2O_3 is difficult to establish, as there are no reliable data for the diffusion of oxygen or aluminum in Al_2O_3 at temperatures within this range. At temperatures where data exist for both aluminum and oxygen, the self-diffusion coefficients for oxygen in single crystals are more than an order of magnitude less than those for aluminum.[26] However, it has been suggested[27] that in polycrystalline samples, although the rate of aluminum diffusion is similar, that of oxygen is enhanced by the presence of grain boundaries, and the self-diffusion coefficients for oxygen

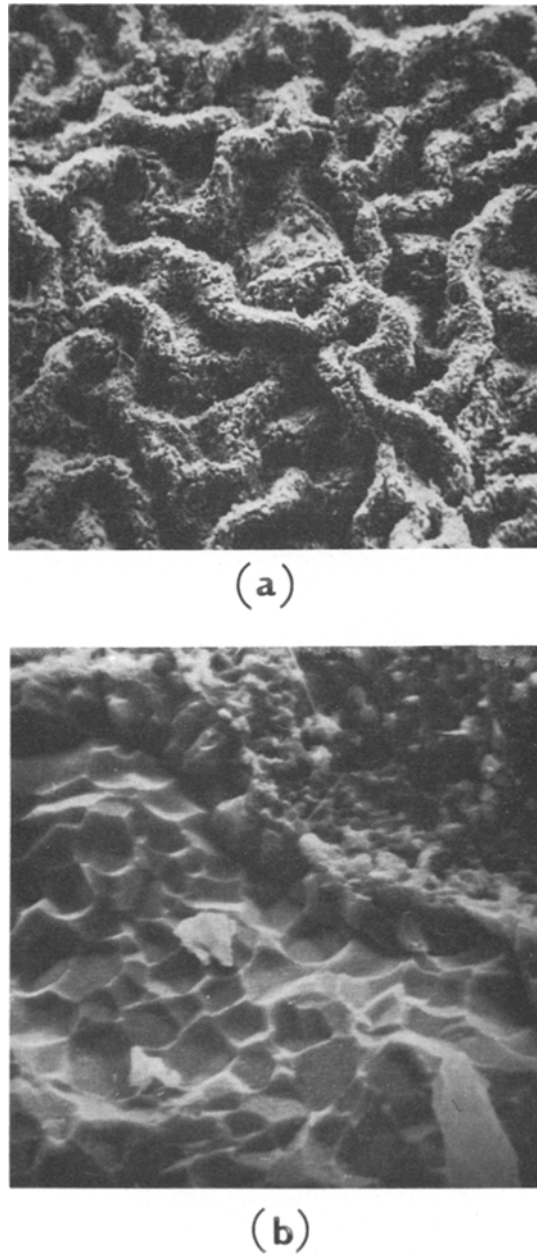

Fig. 22. Co–10Cr–11Al–0.05Hg oxidized for 1000 hr at 1200°C. (a) Surface of scale (×160); (b) alloy surface after partial scale removal (×1600). Both parts reduced 20% for reproduction.

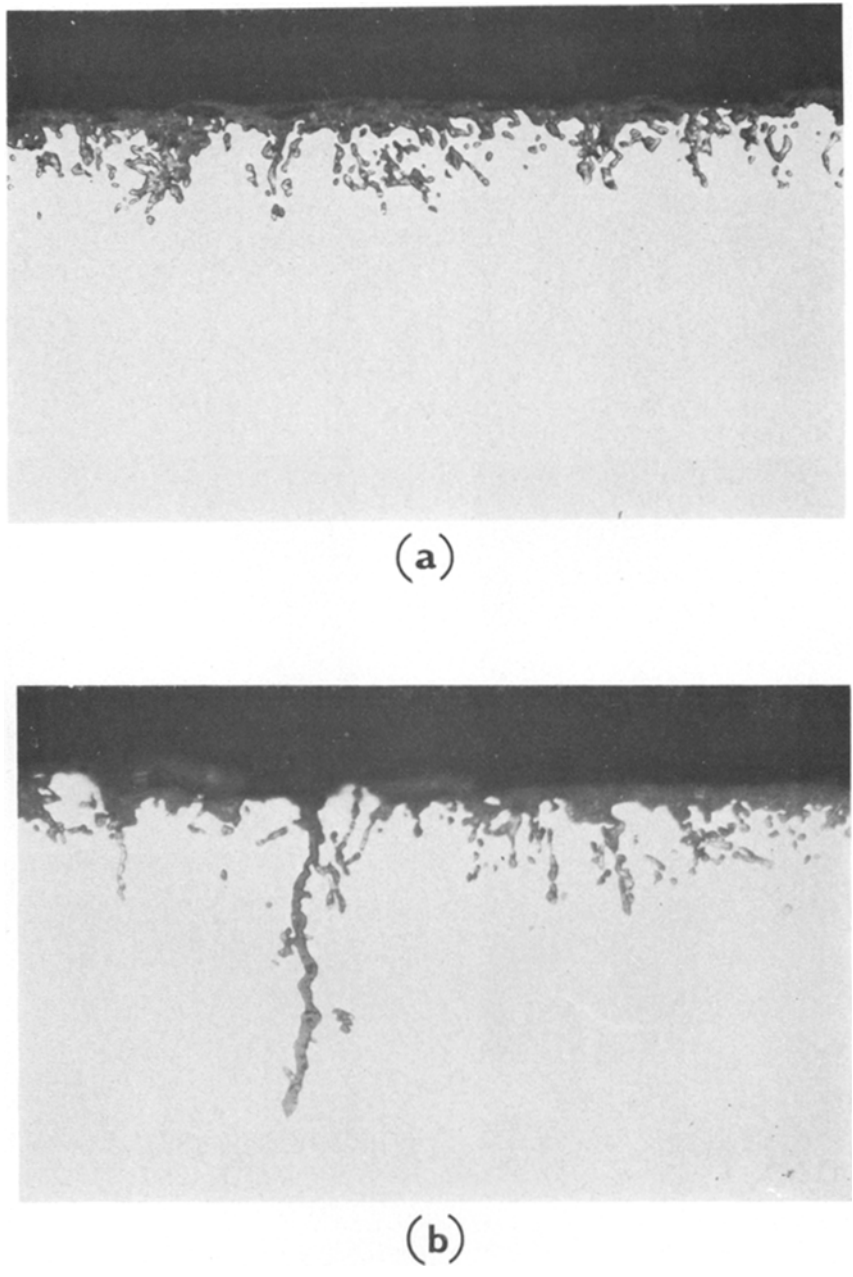

Fig. 23. Cross sections of CoCrAlHf alloys oxidized for 17 20 hr cycles at 1200°C. (a) Co–10Cr–11Al–1Hf (×480); (b) Co–10Cr–7Al–1Hf (×480). Both parts reduced 20% for reproduction.

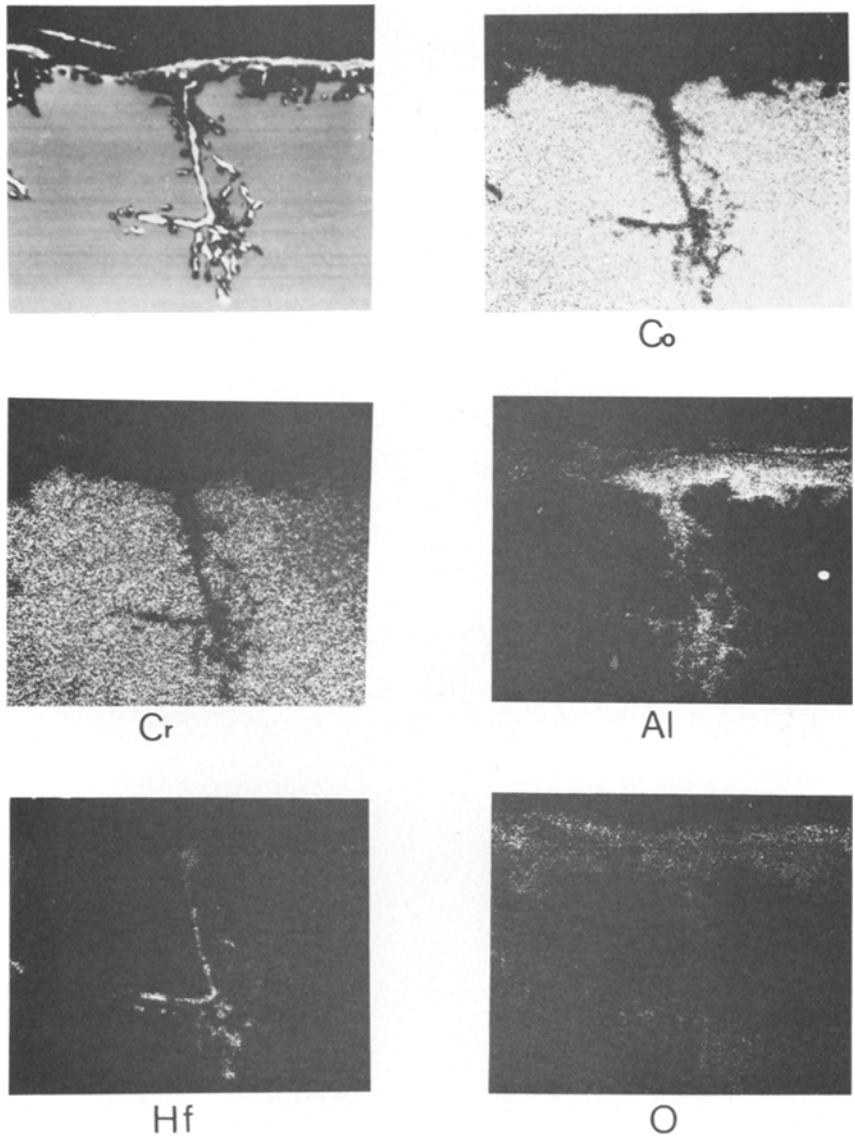

Fig. 24. Electron probe microanalysis of the scale formed on Co–10Cr–7Al–1Hf oxidized for 1000 hr at 1200°C. ×640; reduced 20% for reproduction.

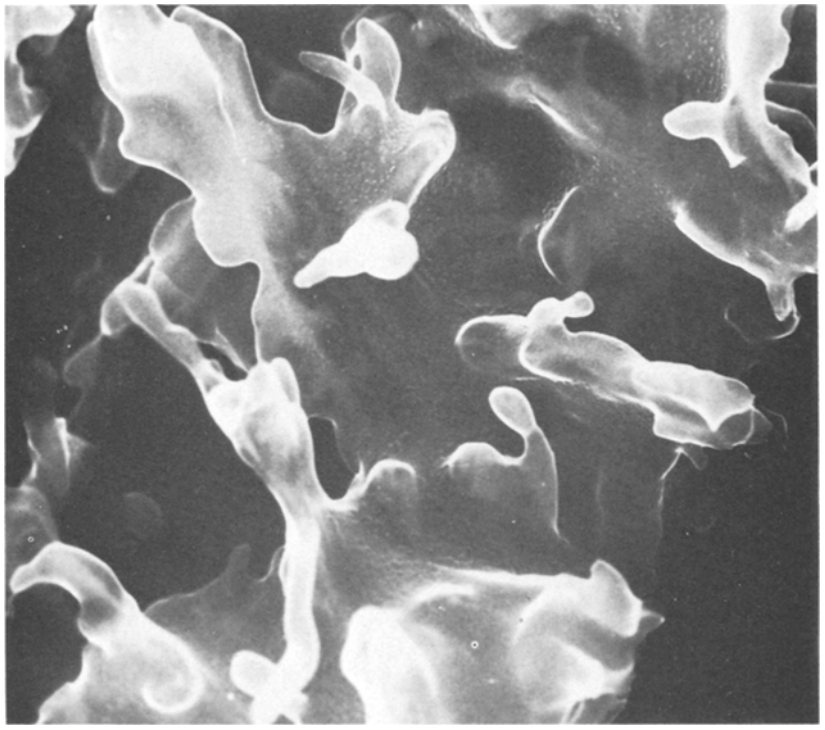

Fig. 25. Underside of the Al_2O_3 scale formed on Co–10Cr–11Al–1Hf oxidized for 1000 hr at 1200°C following dissolution of substrate. ×2400.

are greater than those of aluminum when the grain size of the Al_2O_3 is less than 3 μ.

Giggins and Pettit[19] extrapolated the diffusion data for oxygen in grain boundaries 100 Å wide from the measurement temperature 1650 and 1900°C[28] to 1000 and 1200°C and used these values to calculate a parabolic rate constant for Al_2O_3 growth, where this growth is controlled by oxygen diffusion along grain boundaries. The following assumptions were implicit: (i) the diffusion coefficients at a given temperature are constant; (ii) the grain size of the Al_2O_3 is 1 μ; (iii) the activity of Al at the alloy–scale interface is 0.1; (iv) the oxygen pressure in the gas is 0.2 atm.

The calculated rate constants were 7×10^{-14} and 3×10^{-12} $g^2\cdot cm^{-4}\cdot sec^{-1}$ at 1000 and 1200°C respectively. Interpolating between these values gives 5×10^{-13} $g^2\cdot cm^{-4}\cdot sec^{-1}$ at 1100°C, which would correspond to a weight gain after 100 hr exposure at this temperature of 0.44 $mg\cdot cm^{-2}$. This is near the lowest observed values with the ternary

CoCrAl alloy; the Y- and especially Hf-containing alloys are somewhat lower still.

Neither Hf nor Y is detected to any appreciable level in the Al_2O_3 scales, although it is appreciated that very small impurity levels in Al_2O_3 could significantly alter the self-diffusion coefficients: Al_2O_3 is supposed[29] to exhibit an extrinsic defect structure below 1650°C. Trace levels of Co or Cr may also be significant. However, variation of the grain size of the Al_2O_3 may well be more significant, particularly in view of the above hypothesis that continued growth is primarily by inward short-circuit diffusion of oxygen.

The grain size varies through the scale cross section, ranging from approximately 0.5 μ at the scale–gas interface to 5–10 μ near the oxide–alloy interface. Furthermore, this change is more marked with active metal-containing alloys, and the reduction in Al_2O_3 growth rate could be due to an elimination of some of the short-circuit paths for inward oxygen diffusion. Such a mechanism would also be consistent with the instantaneous oxidation rate decreasing at a rate greater than that required by a parabolic rate law: As the oxidation rate declines, larger grains of Al_2O_3 are formed, resulting in fewer grain boundaries and an even further reduction in rate.

There was no evidence of any concentrations of the reactive elements at the scale–alloy interface for any of the alloys; the "graded seal" model therefore appears to be incorrect. There were no obvious signs of increased scale plasticity, although the absence of whiskers on alloys having other than minimal additions of the active elements might imply reduced growth stresses. There was no evidence of the development of a fine dispersion of internal oxides rich in the reactive elements immediately below the alloy–oxide interface, and no obvious signs of vacancy condensation. However, the presence of the active elements in the alloy did reduce the tendency for voids to form at the alloy–oxide interface, and furthermore they did so at very low concentrations and at very short exposure times, certainly before any significant pegs could have developed. It is possible that the active element atoms themselves could act as vacancy sinks, or that fine internal oxide particles below the limit of resolution of the analytical equipment used could have formed and acted as sinks, but no definite evidence of this was found.

A further factor which may be important is the curtailment of the transient stage of oxidation produced by the active element additions. It is possible that vacancy formation and subsequent development of interfacial voids are confined to this period when the faster-growing CoO is being formed. Thus, with the active element-containing alloys there are fewer vacancies to eliminate. Nevertheless, once formed on the active element-

free alloys, the voids persist. The reappearance of voids after very long exposures on alloys containing small amounts of active elements, but not when the concentration is larger, perhaps implies that there is a continuing supply of vacancies and that the vacancy sinks eventually become saturated.

The main factor contributing to improved scale adhesion is the formation of oxide protrusions penetrating into the alloy. In contrast to earlier models, however, the protrusions or pegs are not the oxide of the reactive element, but Al_2O_3 which has grown inwards encapsulating the particles of oxide of the reactive element. The formation of these stringers makes a significant contribution to the overall weight gain, and thus under isothermal conditions, where scale spallation is not very severe, the alloy with the lowest Hf content and the fewest number of these stringers is the most resistant. The concentration of oxide stringers is not as dependent on the Y concentration in the Y-containing alloys. Furthermore, in the 0.1% Y alloy, there are not sufficient numbers present to completely eliminate multilayer scale formation as a contributory factor to the overall weight gain.

Under thermal cycling conditions, again two factors appear to be important. First, the presence of Hf or Y in the alloy, and the resulting formation of oxide protrusions into the alloy at the scale–alloy interface lessens the likelihood of scale spallation. The number of stringers is important, and there are not sufficient in the alloys containing 0.05 and 0.1% Hf; 0.3 and 1.0% Hf additions appear to be the optimum. Furthermore, Hf seems more efficient than Y and this is related to the shape of the pegs as much as to the concentration. With the Hf additions, the internal growth of the Al_2O_3 around the Hf-rich internal oxide particles takes on a branched, dendritic form (Fig. 25) as opposed to the relatively smooth interface between the Al_2O_3 surrounding the Y-rich particles and the alloy. These differences may well be related to the distribution of the active element in the original alloy. Y tends to segregate to grain boundaries as an intermetallic yttride; Hf is completely in solid solution, and this leads to a very fine distribution of small internal oxide precipitates which then promote the branching growth of Al_2O_3 around them. There is also some evidence to suggest that enrichment of Y may occur in the internal oxide zone promoting growth of larger particles; this does not seem to be the case with Hf.

Thus, small pegs seem to be the best, preferably fairly densely distributed; large pegs, in fact, appear to be capable of initiating scale failure themselves.

The second possible factor contributing to the improved resistance to thermal cycling promoted by the active element addition is related to the lower overall growth rate of the Al_2O_3. This means that there is less depletion of aluminum from the alloy surface, and thus a greater chance of Al_2O_3 re-forming if scale loss occurs.

In conclusion, then, Hf seems preferable as an active element addition. The distribution of pegs is far more uniform and few large ones form. Alloys containing 0.3 or 1.0 wt.% Hf were the best of all the alloys examined for cyclic oxidation resistance; under less severe conditions, such as isothermal exposure, the 0.05 and 0.1 wt.% Hf alloys are better since the formation of fewer pegs means there is less localized thickening of the Al_2O_3 scale.

ACKNOWLEDGMENTS

This work was initiated under the sponsorship of the Cobalt Information Centre and completed with the support of the University of Liverpool.

REFERENCES

1. G. R. Wallwork and A. Z. Hed, *Oxid. Met.* **3**, 229 (1971).
2. C. S. Giggins and F. S. Pettit, *Metall. Trans.* **3**, 1071 (1971).
3. H. H. Davis, H. C. Graham, and I. V. Kvernes, *Oxid. Met.* **3**, 431 (1971).
4. M. S. Seltzer, B. A. Wilcox, and J. Stringer, *Metall. Trans.* **3**, 2391 (1972).
5. J. Stringer, B. A. Wilcox, and R. I. Jaffee, *Oxid. Met.* **5**, 11 (1972).
6. J. Stringer and I. G. Wright, *Oxid. Met.* **5**, 59 (1972).
7. I. G. Wright and B. A. Wilcox, *Metall. Trans.* **5**, 953 (1974).
8. J. Stringer, A. Z. Hed, G. R. Wallwork, and B. A. Wilcox, *Corros. Sci.* **12**, 625 (1972).
9. I. G. Wright and J. Stringer, *Metallography* **6**, 65 (1973).
10. C. S. Wukusick and J. F. Collins, *Mater. Res. Stand.* **4**, 637 (1964).
11. E. J. Felten, *J. Electrochem. Soc.* **108**, 490 (1961).
12. B. Lustman, *Trans. Am. Inst. Min. (Metall.) Eng.* **188**, 995 (1950).
13. J. K. Tien and F. S. Pettit, *Metall. Trans.* **3**, 1587 (1972).
14. J. Stringer, *Metall. Rev.* **11**, 113 (1966).
15. J. D. Kuenzly and D. L. Douglass, *Oxid. Met.* **8**, 139 (1974).
16. H. Pfeiffer, *Werkst. Korros.* **8**, 574 (1957).
17. J. M. Francis and J. A. Jutson, *Corros. Sci.* **8**, 574 (1968).
18. F. A. Golightly, F. H. Stott, and G. C. Wood, *Oxid. Met.* **10**, 163 (1976).
19. C. S. Giggins and F. S. Pettit, Final Rept. to Aerospace Res. Labs., Wright Patterson AFB, Contract N. F33615-72-C-1702 (1976).
20. G. R. Wallwork and A. Z. Hed, *Oxid. Met.* **3**, 213 (1971); G. N. Irving, D. P. Whittle, and J. Stringer, *Corrosion* **33**, 56 (1977).
21. J. G. Fountain, F. A. Golightly, F. H. Stott, and G. C. Wood, *Oxid. Met.* **10**, 341 (1976).
22. C. W. Price, I. G. Wright, and G. R. Wallwork, *Metall. Trans.* **4**, 2423 (1973).
23. H. Fischmeister, *Mem. Sci. Rev. Metall.* **62**, 211 (1965).
24. J. Stringer, *Corros. Sci.* **10**, 513 (1970).
25. J. K. Tien and F. S. Pettit, *Metall. Trans.* **3**, 1587 (1972).
26. A. E. Paladino and W. D. Kingery, *J. Chem. Phys.* **37**, 957 (1962).
27. R. E. Mistler and R. L. Coble, *J. Am. Ceram. Soc.* **54**, 60 (1971).
28. R. E. Mistler and R. L. Coble, *J. Appl. Phys.* **45**, 1507 (1974).
29. Y. Oishi and W. D. Kingery, *J. Chem. Phys.* **37**, 480 (1962).